Nonlinear beam matching to gas-filled multipass cells

Marc Hanna, Louis Daniault, Florent Guichard, Nour Daher, Xavier Delen, Rodrigo Lopez-Martens, Patrick Georges

Research Article | Vol. 4, No. 2 / 15 February 2021 / OSA Continuum 732

Nonlinear beam matching to gas-filled multipass cells

MARC HANNA,[1,*] LOUIS DANIAULT,[2] FLORENT GUICHARD,[3] NOUR DAHER,[1] XAVIER DÉLEN,[1] RODRIGO LOPEZ-MARTENS,[2] AND PATRICK GEORGES[1]

[1]*Université Paris-Saclay, Institut d'Optique Graduate School, CNRS, Laboratoire Charles Fabry, 91127, Palaiseau, France*
[2]*Laboratoire d'Optique Appliquée, CNRS, Ecole Polytechnique, ENSTA Paris, Institut Polytechnique de Paris, 181 chemin de la Hunière et des Joncherettes, 91120, Palaiseau, France*
[3]*Amplitude Laser, 11 Avenue de Canteranne, Cité de la Photonique, 33600 Pessac, France*
[*]*marc.hanna@institutoptique.fr*

Abstract: Gas-filled multipass cells are an appealing alternative to capillaries to implement nonlinear temporal compression of high energy femtosecond lasers. Here, we provide an analytic expression for stationary beam coupling to multipass cells that takes into account nonlinear propagation. This allows a constant beam size on the mirrors and at the cell waist, thereby making the optical design more accurate, for example to avoid optical damage or significant ionization. The analysis is validated using spatio-temporal numerical simulations of the propagation in a near-concentric configuration. This is particularly important for multipass cells that are operated in a highly nonlinear regime, which is the current trend since it allows a lower number of roundtrips, relaxing the constraint on mirror coatings performance.

1. Introduction

Nonlinear temporal compression [1] is an important technique that allows a lot of flexibility in ultrafast laser design. As an example, it can be used to turn efficient and robust ytterbium-doped materials-based lasers that typically emit pulses of a few hundred of femtosecond into few-cycle sources [2]. When the energy of the pulses to be compressed is above approximately 100 μJ, the nonlinear media of choice used in compression setups are rare gases. Glass capillaries filled with noble gases have been used for 25 years for that purpose, since they allow both beam confinement and large interaction lengths. An alternative solution is to use a gas-filled multipass cell (MPC). These systems have been proposed recently [3,4], and since then a number of experiments have shown excellent performances in a wide variety of input pulse duration, energy, and average power [5–11], particularly in terms of energy transmission.

One of the limits of energy scaling in gas-filled MPCs is that the peak power must be maintained below the critical power of the gas to avoid beam collapse. For any input pulse characteristics, this condition defines a maximum pressure for the particular gas used to fill the MPC, therefore limiting the B-integral per roundtrip. Experimental demonstrations tend to approach this limit, since it was observed that the spatio-spectral homogeneity remains satisfactory even for peak powers above half the critical power [12]. Operating MPCs at high nonlinearity level allows a lower number of roundtrips for a given compression ratio, thereby relaxing constraints on the mirror coatings both in terms of reflectivity and dispersion.

Input beam coupling in gas-filled MPCs is typically matched to the stationary Gaussian beam [13], to ensure a constant beam size evolution from one roundtrip to the next. This is particularly important to avoid damage on the mirrors or excess ionization at the MPC waist. Up to now, the stationary Gaussian beam target used for beam matching has been obtained ignoring the contribution of nonlinear refraction in the gas, which causes oscillations of the beam size over

#418247 https://doi.org/10.1364/OSAC.418247
Journal © 2021 Received 23 Dec 2020; revised 28 Jan 2021; accepted 29 Jan 2021; published 5 Feb 2021

OSA CONTINUUM

the roundtrips upon nonlinear propagation [14]. These oscillations are more pronounced at high nonlinearity, calling for an improved input beam coupling analysis. Although beam matching can be fine-tuned during experiments, starting from the linear stationary beam, to obtain better homogeneity of the beam sizes at the mirrors, an improved understanding of the impact of nonlinearity on the caustic would help to guide this delicate procedure. Here we show that, in the aberrationless approximation, there exists a stationary Gaussian beam even in the presence of the distributed nonlinear refraction of the gas. We provide an analytical formula for optimized nonlinear beam matching to MPCs. We verify with spatio-temporal numerical simulations of the propagation that this nonlinear beam matching indeed results in stationary propagation in a highly nonlinear configuration. In particular, a near concentric MPC is considered, since it typically allows the most compact design at any given input energy level. Finally, a procedure to achieve this nonlinear beam matching experimentally is outlined. We believe that improved understanding and description of the spatial aspects of nonlinear propagation in these MPCs will allow the expansion of their use, in particular for high energy ultrafast laser systems.

2. Properties of the nonlinearly matched beam

Propagation of a continuous wave (CW) Gaussian beam in a homogeneous nonlinear medium with linear refractive index n_0 and nonlinear refractive index n_2 was shown to satisfy modified laws with respect to the linear case [15]:

$$w(z) = w_0\sqrt{1+\sigma\left(\frac{z}{z_R}\right)^2} \tag{1}$$

$$R(z) = z\left(1+\frac{1}{\sigma}\left(\frac{z_R}{z}\right)^2\right), \tag{2}$$

where w is the beam radius at *1/e*, R is the radius of curvature of the wavefront, z is the propagation distance, w_0 is the beam radius at its waist, $z_R = \pi w_0^2/\lambda$ is the linear Rayleigh range, λ and λ_0 are the central wavelength in the medium and in vacuum respectively, and $\sigma = 1 - P/P_{crit}$ is a nonlinear correction factor that depends on the ratio of the beam power P to the critical power for self-focusing $P_{crit} = 3.77\lambda_0^2/8\pi n_0 n_2$ [16]. We consider propagation of such a beam in a nonlinear MPC as depicted in Fig. 1. To obtain the waist w_0 of the stationary beam in the nonlinear regime, we fix the radius of curvature of the nonlinear beam to be equal to the mirror radius of curvature at the mirror location. This yields

$$w_0 = \sqrt{\frac{\lambda L}{2\pi}\sqrt{\sigma\left(\frac{2R_M}{L}-1\right)}}, \tag{3}$$

where R_M is the radius of curvature of the mirrors, and L is the MPC length. As a result of this modified size and propagation characteristics, and following the same reasoning as in [4], the beam-averaged B-integral accumulated over a roundtrip is

$$B = \frac{8\pi n_0 n_2}{\lambda_0^2}\frac{P_{peak}}{\sqrt{\sigma}}\arctan\left(\sqrt{\frac{L}{2R_M - L}}\right). \tag{4}$$

Because the stationary nonlinear beam is both smaller and has a lower divergence than its linear counterpart, we note that the B-integral per pass increases by a factor $1/\sqrt{\sigma}$ compared to the linear propagation approximation. These expressions are valid for a CW beam, and must be adapted to the case of optical pulses.

OSA CONTINUUM

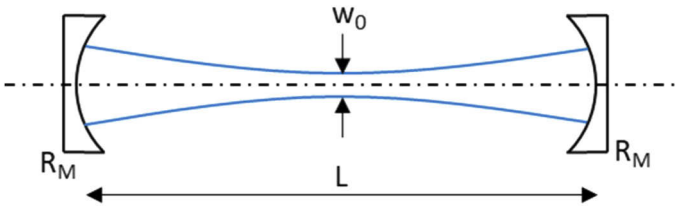

Fig. 1. MPC geometry.

To do this, we use an approach that is equivalent to the concept of effective area in guided-wave nonlinear optics [17]. For a given temporal pulse shape $P(t)$ and energy $E = \int P(t)dt$, we look for the rectangular-shaped pulse that accumulates the same average nonlinear phase $\overline{d\varphi_{NL}}$ in the time domain over a distance dz:

$$\overline{d\varphi_{NL}} = \frac{\int P(t) d\varphi_{NL}(t) dt}{\int P(t) dt}, \tag{5}$$

where $d\varphi_{NL}(t) = \gamma P(t) dz$ is the nonlinear phase accumulated at time t, and γ is the local nonlinear coefficient. This results in the following definition for the effective pulsewidth:

$$\Delta t_{eff} = \frac{(\int P(t)dt)^2}{\int P^2(t)dt}, \tag{6}$$

with a corresponding effective peak power $P_{eff} = E/\Delta t_{eff}$. For a Gaussian pulse with full width at half maximum in power Δt_{FWHM} and peak power P_{peak}, the effective pulsewidth and power are given by

$$\Delta t_{eff} = \sqrt{\frac{\pi}{2\ln(2)}} \Delta t_{FWHM} \qquad P_{eff} = \frac{P_{peak}}{\sqrt{2}}. \tag{7}$$

Just like the effective area allows to take into account spatially averaged nonlinear effects in the time domain, the effective power defined in Eq. (7) allows us to take into account time-averaged nonlinear effects in the spatial domain. Note that these definitions of the effective duration and power are valid for third-order nonlinear effects that can be described as an intensity-dependent index. If we make the assumption that the temporal profile does not change upon propagation, which is verified if dispersion has negligible impact, then beam propagation can be accurately described using the modified Gaussian beam defined by Eqs. (1) and (2), with a nonlinear correction term given by $\sigma = 1 - P_{eff}/P_{crit}$. This time-averaged correction term must also be used in Eqs. (3) and (4) to yield the stationary beam waist and B-integral in the MPC. Note that in Eq. (4), the effective power must be used to compute σ, but the actual peak power must be used in the rest of the expression.

3. Validation with numerical simulations

We now use these results in numerical simulations to assess their validity. Nonlinear propagation is modelled by solving the spatio-temporal nonlinear envelope equation [18], taking into account diffraction, dispersion, and Kerr effects including self-phase modulation, self-focusing, and self-steepening. It is implemented using a split-step Fourier approach [17]. The pulsed beam at a given longitudinal position is described by a two-dimensional field which is a function of time and the radial coordinate, assuming cylindrical symmetry. Transition from the direct space to the Fourier space is achieved using the fast Fourier transform in time and the quasi-discrete Hankel transform [19] in space. The space-time grid for the simulations presented in next sections is as follows: 4 ps time window with 512 points, 7 mm maximum radius for the transverse dimension with 512 points, and a longitudinal step of 2.5 mm.

OSA CONTINUUM

We choose to test the validity of the stationary nonlinear beam matching using simulation parameters approximately matching those of the experimental implementation described in [11], done in a highly nonlinear regime. Perfect Gaussian pulses with a central wavelength of 1030 nm, duration 700 fs, and energy 7 mJ are launched in a MPC filled with 1 bar of argon, corresponding to a nonlinear parameter σ of 0.6. The dispersion and nonlinear index of argon (n_2=0.97×10^{-23} m^2/W at 1 bar) are taken from [20,21]. The MPC mirrors have a radius of curvature of 1 m, a reflection coefficient of 99.5%, and are separated by a length of 1.995 m, slightly detuned from the concentric arrangement into the stability zone. In the linear propagation approximation, this results in a MPC waist of 131 µm, and a beam radius of 2.5 mm on the mirrors. The nonlinear waist given by Eq. (3) is 115 µm.

The evolution of the time-averaged RMS beam radius is plotted in Fig. 2 as a function of the number of passes through the MPC, both on the mirrors and at the MPC waist. Three situations are considered: purely linear propagation as a reference, nonlinear propagation if the beam is launched using linear beam matching, and nonlinear propagation using the nonlinear beam matching procedure described above. When linear beam matching is used, we can clearly observe that nonlinear refraction focuses the beam to a smaller waist, and that the caustic's periodicity is perturbed, causing a progressive decrease of the beam size on the mirrors and an increase at the MPC waist. For this particular case, the decrease in beam size from 2.5 to 1.9 mm corresponds to a fluence multiplied by 1.7, which could cause mirror damage depending on the experimental safety margin. At the waist, the beam radius varies in the range 103–133 µm, which again corresponds to a variation of intensity of a factor 1.7. In contrast, using the nonlinear beam matching condition leads to a stable beam size both at the mirrors and at the focus, with values of 2.18 ± 0.02 mm and 117 ± 1 µm respectively.

Looking in more details, Fig. 3 shows the peak intensity at the MPC waist obtained numerically, which is the quantity that ultimately matters for the ionization limit. Although the beam radius shown in Fig. 2 for the nonlinear beam matching case is almost constant upon propagation, we observe that the peak intensity varies in the range 43 - 64 TW/cm^2, indicating that aberrations lead to beam reshaping away from the perfect Gaussian beam. Still, this intensity variation is much smaller than in the linearly beam matched case, where the intensity is changed by more than a factor 2, over the range 36 - 81 TW/cm^2.

The numerically calculated on-axis B-integral for the first roundtrip is shown in Fig. 4 in the linear and nonlinear beam matching cases. The beam matching does not change the B-integral significantly. This can be understood as follows: it is easy to show that the B-integral accumulated by a Gaussian beam over propagation from minus infinity to plus infinity does not depend on the beam waist [4]. This remains approximately true if the B-integral is computed over a path that includes the beam waist and is much greater than the Rayleigh range, which is the case in a near concentric MPC. This also remains true for the modified nonlinear Gaussian beams used in this paper, which explains that the B-integral per roundtrip is hardly modified, even when the beam sizes at the waist and on the mirrors evolve from one roundtrip to the next.

After a roundtrip, the accumulated B-integral reaches a value of 11.2 rad, corresponding to a beam-averaged value of 5.6 rad for a Gaussian beam, to be compared to the analytical value predicted by Eq. (4) of 4.3 rad, and to the linear propagation approximation (σ=1) value of 3.3 rad. The reason for the discrepancy between the numerically obtained result and the analytical estimate can be traced back to the higher-order spatial phase (aberrations) imparted by the Kerr lens, that leads to a smaller effective area in the vicinity of the beam waist. This is in line with the observations made on the evolution of peak intensity.

Note that the present analysis entirely neglects ionization and plasma–related effects, which are typically avoided in gas-filled MPCs. Indeed, since these phenomena are much more nonlinear than the Kerr effect, their effect result in complete beam breakdown above a threshold that

OSA CONTINUUM

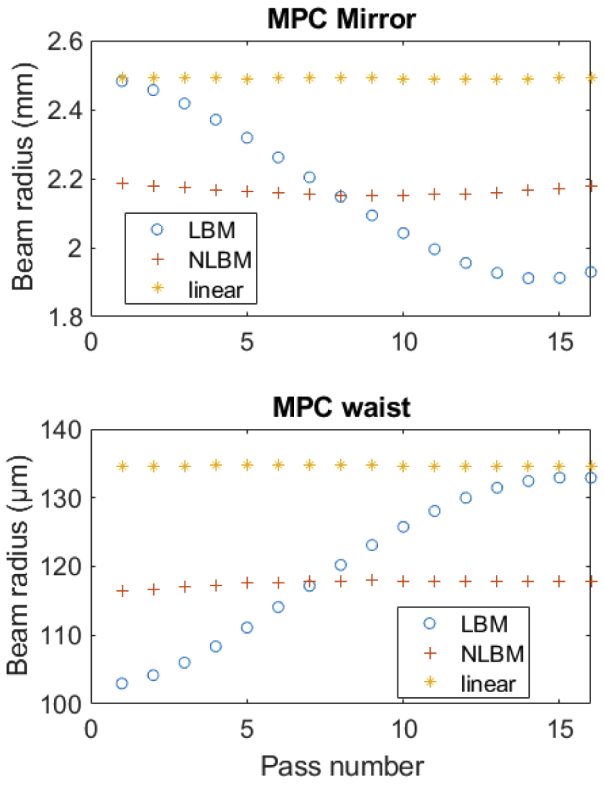

Fig. 2. Time-averaged RMS beam radius sampled at the MPC mirrors (top) and at the MPC center (bottom) as a function of pass number in the MPC in three different cases: linear refers to purely linear beam matching and propagation, LBM refers to linear beam matching and nonlinear propagation, NLBM to nonlinear beam matching and propagation.

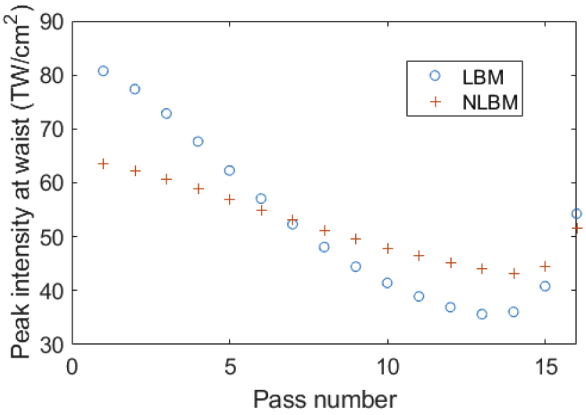

Fig. 3. Peak intensity at the MPC center as a function of pass number in two cases: LBM refers to linear beam matching and nonlinear propagation, NLBM to nonlinear beam matching and propagation.

OSA CONTINUUM

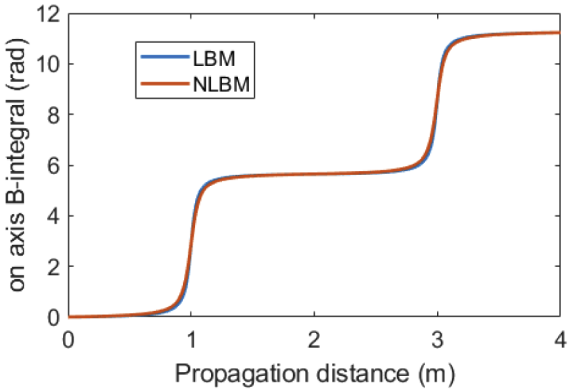

Fig. 4. On-axis B-integral accumulated over the first roundtrip in the MPC. LBM refers to linear beam matching, NLBM to nonlinear beam matching.

corresponds to the onset of significant ionization rate [7], depending on the ionization potential for the considered rare gas.

4. Experimental beam matching procedure

We now discuss how to use this result in practice. Propagation in a gas-filled MPC is modified by nonlinear refraction in the gas as soon as the beam goes through the window that is used to seal the cell. However, mode matching to the cell is often achieved at atmospheric air pressure and at reduced power to facilitate experimental adjustments and diagnostics, resulting in an essentially linear propagation. This can be taken into account using the following procedure. One of the result concerning the nonlinear Gaussian beam described in Eqs. (1) and (2) is that its propagation through an optical system can be easily computed using the standard ABCD matrix method, applied to a modified generalized reduced radius of curvature [15] defined as

$$\frac{1}{\widetilde{q_{NL}}} = \frac{n_0}{R} + i\sqrt{\sigma}\frac{\lambda_0}{\pi w^2}. \tag{8}$$

In order to determine what the optimal beam waist and location are in the absence of nonlinear gas, one should therefore start from the MPC center with the optimal nonlinear beam size given by Eq. (3), and propagate the beam back through the optical system to the entrance window using the nonlinear $\widetilde{q_{NL}}$ parameter corresponding to the expected peak power and gas nature and pressure. From the entrance window, the beam can then be linearly propagated ($\sigma = 1$) towards the MPC center to reveal the target beam waist and position to be used during the beam matching procedure.

As an example, let us consider the case of the MPC described in section 3. If we assume that, from the input window, the beam first propagates over 1 m, then is focused into the MPC waist by a f=1 m lens or mirror, the waist radius that should be aimed for in the absence of gas is 150 µm, in order to reach the optimal waist size of 115 µm in the presence of gas. In this configuration, the waist position is unchanged by nonlinear refraction, but it is not always the case. This illustrates the practical importance of the present study for experimental implementations of highly nonlinear MPCs.

5. Conclusion

As a conclusion, we derive the stationary condition for a symmetric MPC in the nonlinear aberrationless Gaussian beam approximation. The notion of effective power allows to easily

OSA CONTINUUM

account for the pulsed nature of beams. This analysis is checked using spatio-temporal numerical simulations, validating the fact that nonlinear refraction should be taken into account to optimize coupling in highly nonlinear MPCs.

Although we have restricted the analysis to gas-filled cells, nonlinear propagation using ABCD matrices and the $\widehat{q_{NL}}$ parameter could be used to perform the same analysis in MPCs that include plates of bulk material. This formalism can also be used to guide experimental design of optical systems for input and output coupling of gas-filled capillary setups. Overall, we believe that these results will be helpful in designing future high energy MPCs for temporal compression of high energy laser sources.

Funding. Agence Nationale de la Recherche (ANR-10-LABX-0039-PALM, ANR-16-CE30-0027-01-HELLIX, ANR-19-CE30-0001-02-MIRTHYX).

Disclosures. The authors declare no conflicts of interest.

References

1. M. Nisoli, S. De Silvestri, O. Svelto, R. Szipöcs, K. Ferencz, C. Spielmann, S. Sartania, and F. Krausz, "Compression of high-energy laser pulses below 5 fs," Opt. Lett. **22**(8), 522–524 (1997).
2. L. Lavenu, M. Natile, F. Guichard, X. Délen, M. Hanna, Y. Zaouter, and P. Georges, "High-power two-cycle ultrafast source based on hybrid nonlinear compression," Opt. Express **27**(3), 1958–1967 (2019).
3. J. Schulte, T. Sartorius, J. Weitenberg, A. Vernaleken, and P. Russbueldt, "Nonlinear pulse compression in a multi-pass cell," Opt. Lett. **41**(19), 4511–4514 (2016).
4. M. Hanna, X. Délen, L. Lavenu, F. Guichard, Y. Zaouter, F. Druon, and P. Georges, "Nonlinear temporal compression in multipass cells: theory," J. Opt. Soc. Am. B **34**(7), 1340–1347 (2017).
5. M. Ueffing, S. Reiger, M. Kaumanns, V. Pervak, M. Trubetskov, T. Nubbemeyer, and F. Krausz, "Nonlinear pulse compression in a gas-filled multipass cell," Opt. Lett. **43**(9), 2070–2073 (2018).
6. L. Lavenu, M. Natile, F. Guichard, Y. Zaouter, X. Delen, M. Hanna, E. Mottay, and P. Georges, "Nonlinear pulse compression based on a gas-filled multipass cell," Opt. Lett. **43**(10), 2252–2255 (2018).
7. M. Kaumanns, V. Pervak, D. Kormin, V. Leshchenko, A. Kessel, M. Ueffing, Y. Chen, and T. Nubbemeyer, "Multipass spectral broadening of 18 mJ pulses compressible from 1.3 ps to 41 fs," Opt. Lett. **43**(23), 5877–5880 (2018).
8. P. Russbueldt, J. Weitenberg, J. Schulte, R. Meyer, C. Meinhardt, H. D. Hoffmann, and R. Poprawe, "Scalable 30 fs laser source with 530 W average power," Opt. Lett. **44**(21), 5222–5225 (2019).
9. C. Grebing, M. Müller, J. Buldt, H. Stark, and J. Limpert, "Kilowatt-average-power compression of millijoule pulses in a gas-filled multi-pass cell," Opt. Lett. **45**(22), 6250–6253 (2020).
10. P. Balla, A. Bin Wahid, I. Sytcevich, C. Guo, A.-L. Viotti, L. Silletti, A. Cartella, S. Alisauskas, H. Tavakol, U. Grosse-Wortmann, A. Schönberg, M. Seidel, A. Trabattoni, B. Manschwetus, T. Lang, F. Calegari, A. Couairon, A. L'Huillier, C. L. Arnold, I. Hartl, and C. M. Heyl, "Postcompression of picosecond pulses into the few-cycle regime," Opt. Lett. **45**(9), 2572–2575 (2020).
11. P. L. Kramer, M. K. R. Windeler, K. Mecseki, E. G. Champenois, M. C. Hoffmann, and F. Tavella, "Enabling high repetition rate nonlinear THz science with a kilowatt-class sub-100 fs laser source," Opt. Express **28**(11), 16951–16967 (2020).
12. N. Daher, F. Guichard, S. W. Jolly, X. Délen, F. Quéré, M. Hanna, and P. Georges, "Multipass cells: 1D numerical model and investigation of spatio-spectral couplings at high nonlinearity," J. Opt. Soc. Am. B **37**(4), 993–999 (2020).
13. A. E. Siegman, "*Lasers*," (University Science Books, 1986).
14. M. Hanna, N. Daher, F. Guichard, X. Délen, and P. Georges, "Hybrid pulse propagation model and quasi-phase-matched four-wave mixing in multipass cells," J. Opt. Soc. Am. B **37**(10), 2982–2988 (2020).
15. P.-A. Belanger and C. Pare, "Self-focusing of Gaussian beams: an alternate derivation," Appl. Opt. **22**(9), 1293–1295 (1983).
16. A. Couairon, E. Brambilla, T. Corti, D. Majus, O. de J. Ramırez-Gongora, and M. Kolesik, "Practitioner's guide to laser pulse propagation models and simulation," Eur. Phys. J. Spec. Top. **199**(1), 5–76 (2011).
17. G. P. Agrawal, "*Nonlinear fiber optics*," 5th edition, (Academic Press, 2012).
18. T. Brabec and F. Krausz, "Nonlinear optical pulse propagation in the single-cycle regime," Phys. Rev. Lett. **78**(17), 3282–3285 (1997).
19. M. Guizar-Sicairos and J. C. Gutiérrez-Vega, "Computation of quasi-discrete Hankel transforms of integer order for propagating optical wave fields," J. Opt. Soc. Am. A **21**(1), 53–58 (2004).
20. A. Bideau-Mehu, Y. Guern, R. Abjean, and A. Johannin-Gilles, "Measurement of refractive indices of neon, argon, krypton, and xenon in the 253.7-140.4 nm wavelength range. Dispersion relations and estimated oscillator strengths of the resonance lines," J. Quant. Spectrosc. Radiat. Transfer **25**(5), 395–402 (1981).
21. J. K. Wahlstrand, Y.-H. Cheng, and H. M. Milchberg, "High Field Optical Nonlinearity and the Kramers-Kronig Relations," Phys. Rev. Lett. **109**(11), 113904 (2012).